ARTICLE

Synthesis and Electrocatalytic Activity of Photoreduced Platinum Nanoparticles in a Poly(ethylenimine) Matrix

Litao Bai, Huizhen Zhu, Joseph S. Thrasher, and Shane C. Street*

Department of Chemistry, The University of Alabama, Tuscaloosa, Alabama 35487-0336

ABSTRACT Monodisperse polymer-mediated platinum (Pt) nanoparticles (NPs) have been synthesized by photoreduction in the presence of poly(ethylenimine) (PEI), a hyperbranched polymer. The formation process of the Pt NPs is pursued by UV−vis spectroscopy, and the formation mechanism is discussed. The morphology and size of the Pt NPs were characterized by transmission electron microscopy (TEM). TEM imaging shows that the Pt NPs' average diameter is 2.88 ± 0.53 nm. The PEI/Pt NPs were immobilized on glassy carbon electrodes, and the electrocatalytic activity of the catalysts was investigated by cyclic voltammetry. PEI/Pt NPs exhibit very high catalytic activity for a methanol oxidation reaction. PEI/Pt NPs on glassy carbon electrodes are robust, showing good tolerance to poisoning even after many cycles. The electrocatalytic activity of PEI/Pt NPs compares favorably with other polymer-mediated Pt NPs. The results indicate that PEI is an appropriate complexing reducing agent for the photochemical production of Pt NPs and a good capping agent, allowing immobilization of the NPs on the working electrode.

KEYWORDS: Pt nanoparticles • photoreduction • formation mechanism • poly(ethylenimine) • electrocatalytic activity • methanol oxidation

1. INTRODUCTION

Direct methanol fuel cells (DMFCs) using liquid methanol are promising candidates for future power sources to compete with conventional batteries in portable electronic devices because of their high energy conversion efficiency, low operation temperatures, and low pollutant emission (1). Methanol as a fuel has advantages compared to, say, hydrogen: it is cheap, easily handled, transported, and stored, and has high energy density (2). Although progress has been made in the development of DMFCs, practical applications still face severe performance and durability challenges (3) because of the poor electrocatalyst performance (4) at both the anode and cathode and the crossover of methanol (5) from an anode to a cathode through the proton-exchange membrane. The slow kinetics of the oxygen reduction reaction (ORR) (6), which is responsible for an overpotential loss of ∼0.3−0.4 V under typical conditions of operation, and poor methanol electrooxidation reaction kinetics (7) also seriously affect the DMFC performance. The development of a DMFC requires a broad search for catalytic materials for better electrocatalysts to reduce the overpotential and improve the cell performance (8). Among various alternative candidates, platinum (Pt) and Pt-based alloy catalysts are the best catalysts (to date) for both the ORR at the cathode and methanol oxidation reaction (MOR) at the anode (8−10), but even with the Pt-based catalysts, the activity is still not high enough. This drives the use of a high Pt loading, thus increasing cost and limiting sustainability, barriers to the commercial application of DMFCs. For eventual widespread application of DMFCs, material costs will need to be lowered while the performance and reliability are improved. An effective way to lower the cost of the catalyst is to reduce the amount of Pt used in DMFCs without sacrificing the performance.

The particle shape and size (11) as well as dispersion are key factors that determine Pt-based catalysts' ORR activity and cell performance for DMFCs (12, 13). Small and uniform Pt nanoparticles (NPs) with high surface-to-volume ratios are preferred to achieve a reliable catalytic performance and to increase the efficiency. The active surface area of the catalyst can be greatly increased by reducing the size of the Pt NPs and therefore creating a larger number of catalytically active centers. Therefore, the synthesis of a Pt nanomaterial with specific morphology (14) and controlled size is of great importance in the practical synthesis of Pt particles (15). Substantial effort has been devoted to the development of new synthetic methodologies of Pt catalysts (16), especially in the diameter range of 2−10 nm, to improve the catalytic performance (17).

A number of chemical routes have been employed to synthesize Pt nanomaterials with controlled size and catalytic properties, such as the use of chemical reductants in aqueous (16) and organic-phase solvents (18), electrochemical approaches (19), thermal reduction (20), sonochemical methods (21), radiolytic (22), microwave (23), and photochemical methods (24), etc. Chemical methods with $NaBH_4$ as the reductant for the preparation of Pt NPs are convenient, but the quantity of Pt NPs is dependent on, for example, solution conditions, the rate and sequence of reductant addition, and the local overconcentration of reductants (25). It can be difficult to produce monodisperse

* Fax: 205-348-9104. E-mail: sstreet@bama.ua.edu.
Received for review July 14, 2009 and accepted September 13, 2009
DOI: 10.1021/am900471f
© 2009 American Chemical Society

Published on Web 10/01/2009

NPs with controlled morphology by these methods. Furthermore, excess reducing agents and their oxidation products may contaminate the final product. To synthesize size-controlled Pt particles, photochemical methods have shown some promise (26). Colloidal dispersion of Pt particles has been obtained through the photoreduction of Pt complexes in the presence of a protective polymer under mild and controllable conditions. The photoreduction of Pt complexes is attractive because (i) large numbers of Pt nuclei are homogeneously and instantaneously produced, so the reduction reaction arises uniformly in the solution and, thus, the size of the final NPs is very uniform, (ii) controlled reduction of the metal ions can be carried out without using excess reducing agent, and no adsorbing contamination on the product occurs in the preparation process, and (iii) the photochemical method can be cost-effective and convenient. A number of studies have focused on the synthesis of Pt particles by photochemical reduction methods. In 2005, Harada and Einaga (24) used poly(*N*-vinyl-2-pyrrolidone) (PVP) as a stabilizer in a water/ethanol solution and synthesized Pt NPs by UV radiation, and the formation mechanisms were discussed. Their research showed that this process is a promising method to prepare small Pt NPs with a narrow particle size distribution, which can be easily deposited on a substrate and shows high catalytic activity for CO photooxidation. In most cases, photoreduction from Pt precursors to the metal only takes place in the presence of alcohol; i.e., alcohol is the (source of) reducing agent under UV irradiation (26). However, Luo and Imae (27) showed that, by using poly(amidoamine) (PAMAM) dendrimers as stabilizers, Pt ions can be photoreduced to Pt NPs in water, although the reaction mechanism was not identified. The problem with this system is that PAMAM is very expensive and requires complex preparation prior to use. Also, the Pt NPs prepared by this method only show a crown shape with a size range of 100−130 nm because of PAMAM aggregation under the solution conditions used.

Pt NP preparation methods involve the reduction of Pt ions into NPs in protective media to prevent the metal NPs from aggregating. Water-soluble polymers such as poly(vinyl alcohol) (28) and PVP (29) have been widely used as protective media for colloidal dispersions. Stabilizers play an important role in controlling the formation of NPs as well as their dispersion stability. On the other hand, the presence of too strong a capping agent on the NP surfaces can limit the particles' catalytic activity. For example, PVP-capped Pt NPs do not show any electrocatalytic activity toward oxygen reduction or methanol oxidation because of the strong affinity of PVP for Pt (29).

Poly(ethylenimine) (PEI) is a hydrophilic polymer with primary, secondary, and tertiary amino groups and an overall positive charge in the neutral aqueous solution. Because of its abundant positive charge, it is a widely used stabilizer in the coating of NPs to achieve surface functionalization (30). The positively charged amine groups stabilize NPs in solution and can also be used to form self-assembled monolayers on common electrodes. Laschi et al. (31) developed glassy carbon electrodes modified with a dispersion of multiwall carbon nanotubes (CNTs) in PEI. These exhibit excellent electrocatalytic activity toward several analytes. PEI contains one of the highest densities of amine groups among all polymers, supporting the highly efficient dispersion of NPs in PEI as well as the high electroactivity of PEI/CNTs immobilized on the electrode surface (32). At the same time, PEI can be used as a reducing agent in the preparation of metal NPs. For example, Sun et al. (33) prepared PEI-protected gold NPs by heating of an PEI/$HAuCl_4$ aqueous solution. In their experiment, PEI serves both as a reducing agent and a protective capping agent.

Polyelectrolyte-capped Pt NPs can be synthesized in aqueous solution, and their assembly on electrodes can allow control of the size, distribution, shape, and surface density (34). Pan et al. (35) demonstrated membrane-electrode assembly of polymer electrolyte fuel cells prepared using charged Pt NPs with an ultralow Pt loading. Estephan et al. (36) showed that nanostructured Pt electrodes were assembled from solution-prepared polyacrylate-capped Pt NPs by virtue of electrostatic and hydrophobic interactions with a cationic polyelectrolyte: poly(diallyldimethylammonium) chloride. Electrochemical characterization of the polyelectrolyte-stabilized Pt NPs showed that these surfaces are catalytically active for reactions including oxygen reduction, methanol oxidation, and hydrogen oxidation (37).

We present here a simple, clean, and efficient route to preparing PEI/Pt NPs. PEI/Pt NPs were prepared by a two-step procedure. First, PEI and $PtCl_6^{2-}$ ions are mixed with the desired ratio. $PtCl_6^{2-}$ will complex with functional groups on PEI in an aqueous solution. Then, UV irradiation results in the conversion of $PtCl_6^{2-}$ to Pt^0 NPs. PEI/Pt NPs with an average diameter of about 3 nm were prepared. The mechanism for the photoreduction of PEI-mediated $PtCl_6^{2-}$ to give Pt NPs in aqueous solution was also studied. Our research shows that this process is a good method to prepare small Pt NPs with a narrow particle size distribution. The PEI/Pt NPs were subsequently deposited on glass carbon electrodes and the electrocatalytic activities investigated. The Pt NPs immobilized on the glass carbon electrode show excellent electrocatalytic activity and stability.

2. EXPERIMENTAL METHODS

2.1. Materials. Hexachloroplatinum(IV) acid hydrate ($H_2PtCl_6 \cdot 6H_2O$; guaranteed reagent) was obtained from Fisher Chemical Company. Poly(ethylenimine) (PEI) with a weight-average molecular weight of 25 000 was purchased from Aldrich. Sulfuric acid (H_2SO_4, 99.99%) and methanol (CH_3OH, anhydrous) were analytical grade. All chemicals were used as received without further purification. The 18 M$\Omega \cdot$ cm resistivity water was obtained from a Millipore water purifier. The concentration of the polymer solution is based on the monomer unit.

A Rayonet photochemical reactor (model RPR-600, Southern New England Ultraviolet Inc.) was used as a UV-irradiation system in our experiments. The photochemical reactor is supplied with eight 253.7 nm light sources (8 W per lamp), equipped with a merry-go-round unit that holds samples for equal irradiation at one time at 5 rpm, and a cooling fan keeps the temperature at ambient.

2.2. Synthesis of PEI/Pt NPs. Colloidal dispersions of Pt NPs were synthesized from H_2PtCl_6 complexed with PEI by UV irradiation. In a typical procedure, 0.3 mL of 10 mM H_2PtCl_6 was added to 2.55 mL of a PEI aqueous solution (20 mM C_2H_5N monomer concentration). The typical final molar ratio of PEI/$PtCl_6^{2+}$ was 17. The resulting solution was diluted to 5 mL with deionized water and then was bubbled with nitrogen to remove dissolved oxygen and complete the formation of the $PtCl_6^{2-}$/PEI complex in quartz tubes. Under these experimental conditions, the initial reaction mixtures were yellowish in color. The yellow solution in quartz tubes was placed in a photochemical reactor and irradiated by 254 nm light. The samples were irradiated for 1 day. The growth of Pt NPs was monitored at different intervals using UV−vis absorption spectroscopy.

2.3. Characterization of PEI/Pt NPs. Transmission electron microscopy (TEM) images of Pt NPs were obtained from a transmission electron microscope (FEI TECNAI F20). The electron beam acceleration voltage was set at 200 kV. Images were obtained by deposition of a drop of solution onto a carbon-coated 300 mesh copper grid resting on absorbent filter paper, which rapidly wicked away the water and allowed the NPs to be dispersed on the grid, followed by air-drying under ambient conditions. All images were digitally recorded with a CCD camera (1024 × 1024 pixels), and image processing was carried out using a Digital Micrograph and Digimizer (Gatan). Histograms of the particle size distribution and average diameter were obtained by measuring 300 particles in chosen areas enlarged in a Digimizer. The UV−vis absorption spectra of the NP solution were measured by a Cary 50 UV−vis spectrophotometer (Varian, USA) using a 1 cm optical path length quartz cuvette to pursue the reaction in solution.

2.4. Immobilization of PEI/Pt NPs on Glassy Carbon Electrodes. Glassy carbon electrodes were used as substrates for the immobilization of Pt NPs. The glassy carbon working electrode with a geometrical surface area of 0.07 cm^2 was polished with 1 and 0.05 μm Al_2O_3 powders successively on a Nanocloth, followed by sonication in deionized water. PEI/Pt NP solutions prepared by UV irradiation were pipetted onto the surface of the glassy carbon electrode. After water was evaporated overnight at room temperature, the PEI/Pt NP coating was irradiated for 1 h in the Rayonet photochemical reactor. Then the electrode was washed carefully with ultrapure water before measurement.

2.5. Electrochemical Instrumentation and Measurements. All electrochemical measurements were performed in a conventional three-electrode cell at room temperature. A Pt wire was used as a counter electrode. All electrochemical potentials in the present study are given versus a Ag/AgCl (saturated KCl) reference electrode. The working electrode was a PEI-mediated Pt-coated glassy carbon electrode (diameter 3 mm). In order to minimize the effects of impurities during the measurements, the electrode was cycled in a 1 M H_2SO_4 solution at 50 mV s^{-1} between 0 and 1.2 V until reproducible cyclic voltammograms were obtained prior to any electrochemical measurements. Cyclic voltammograms and chronoamperometry were recorded using a computer-controlled CHI 660 electrochemical workstation (CH Instruments, Austin, TX). Hydrogen adsorption cyclic voltammograms were recorded in a nitrogen-protected 1 M sulfuric acid aqueous solution. The solution was purged with nitrogen to deplete dissolved oxygen before each run. The region for hydrogen adsorption was used to estimate the electrochemically active surface areas. Fresh 1 M H_2SO_4 + 2 M CH_3OH was used in every methanol electrooxidation methanol measurement to get reliable and reproducible results.

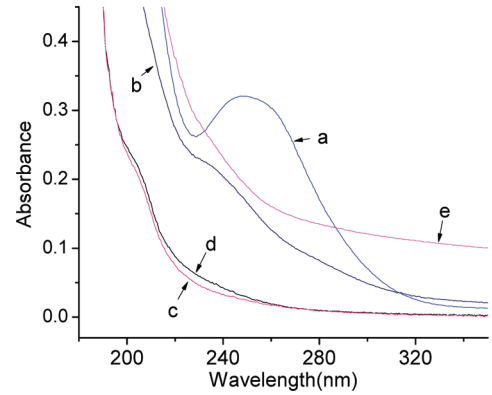

FIGURE 1. Variation of UV−vis absorption spectra during the photoreduction of H_2PtCl_6: (a) H_2PtCl_6 aqueous solution; (b) mixture of H_2PtCl_6 with PEI; (c) complex of H_2PtCl_6 with PEI after 5 min of UV irradiation; (d) complex of H_2PtCl_6 with PEI after 60 min of UV irradiation; (e) complex of $H_2PtCl_6$with PEI after 1 day of UV irradiation.

3. RESULTS AND DISCUSSION

3.1. Preparation and Characterization of PEI/Pt NPs. ***Synthesis of PEI/Pt NPs.*** It is well-known that transition-metal colloids can be formed by photochemical reactions in water/alcohol solutions, in which the reduction of metal salts takes place by solvated electrons and free radicals produced under irradiation. The photochemistry of Pt complexes has been widely investigated in the past because of the virtue of slow and controllable photoreduction processes to produce small and well-dispersed Pt NPs. Methanol is the reducing agent under UV irradiation in most cases of Pt photoreduction (38). It is suggested that organic free radicals are produced from adsorbed methanol under UV irradiation and the radicals reduce Pt salts (39). In this investigation, a photoreduction method was performed to synthesize colloidal Pt NPs by the reduction of $PtCl_6^{2-}$ in a PEI aqueous solution without ethanol. PEI was used as both the stabilizer and the reducing agent.

Absorption Spectra. $PtCl_6^{2-}$ aqueous solutions are yellow in color. When $PtCl_6^{2-}$ is mixed with PEI, the yellow color becomes less intense. Irradiating with UV light for a few minutes changes the solution color to orange, which is the typical color of $PtCl_4^{2-}$. Then the solution changes to dark brown slowly with further UV irradiation. This process of PEI-mediated Pt colloidal synthesis via the photoreduction of $PtCl_6^{2-}$ was followed by UV−vis spectroscopy. Figure 1 presents the UV−vis spectra of the Pt solutions with PEI and without PEI before and after UV irradiation in dilute solution. Figure 1a shows a typical electronic absorption spectrum of H_2PtCl_6 in aqueous solution, which displays a strong absorption band in 250 nm. After mixing with PEI, as shown in Figure 1b, the peak at 250 nm disappears, and a new shoulder peak at 235 nm appears because of ligand-to-metal charge transfer (40), which is assigned to the absorption band of a complex of $PtCl_6^{2-}$ with PEI (chloride ligands were replaced by the amine groups of PEI). After only 5 min of irradiation, the peak at 235 nm totally disappears, and another shoulder peak at 210 nm appears, as shown in Figure 1c. This is typical of the absorption by $PtCl_4^{2-}$ (41). We conclude that Pt^{4+} was reduced to Pt^{2+} in the first 5 min,

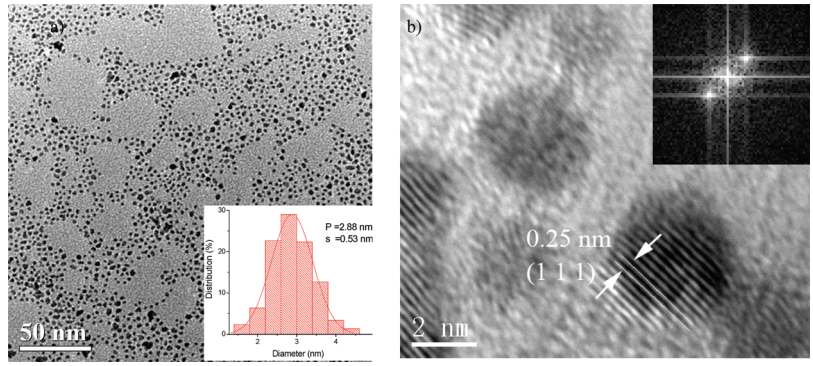

FIGURE 2. TEM images of PEI/Pt NPs synthesized by photoreduction. (a) Image in moderate magnifications. The inset at the bottom shows the corresponding size distribution histograms of PEI/Pt NPs. (b) HRTEM of Pt NPs. The inset on the top right shows the FFT pattern. The fringe spacing of 0.25 nm corresponds to the interplanar separation between the (111) planes.

a fast reaction. Curve d in Figure 1 shows the adsorption of the solution after 60 min of irradiation. The spectra of the solutions irradiated for 60 min are similar to the solution irradiated for 5 min, with only a small increase in the 210 nm feature and a slightly increased baseline compared with curve c. Apparently, no further reduction of Pt^{2+} occurs until almost all of Pt^{4+} is reduced to Pt^{2+}. The further reduction of Pt^{2+} to Pt^0 is a slow process compared with the reduction of Pt^{4+} to Pt^{2+}. This is consistent with Cameron's NMR observation of the photoreduction of Pt in an ethanol/water solution (42). Cameron indicated that the photoreduction of $PtCl_6^{2-}$ complexes to Pt^0 via Pt^{2+} and Pt^0 metal formation does not occur until a ~90% yield of $PtCl_4^{2-}$ has accumulated. Photoirradiation for 1 day resulted in the complete disappearance of the absorption band and a significant increase of the baseline absorbance. The spectrum of the solution after 1 day of UV irradiation is presented in curve e, which implies the formation of Pt NPs (27). This feature has been observed for PVP-stabilized Pt by photoreduction and heat treatment in an alcohol/water solution and hydrogen reduction in water, indicating that $PtCl_6^{2-}$ complexes were reduced to metallic species (39). (XPS spectra of as-made Pt NPs also confirmed the metallic Pt species. See Figure S1 in the Supporting Information.) The resulting solution was stable, and no large aggregates or precipitates were observed for at least several months.

TEM Images and Size Distributions. Figure 2a shows a typical TEM image at moderate magnification and the corresponding size distribution histograms of the PEI/Pt NPs after photoirradiation. The average particle diameter is 2.88 ± 0.57 nm. The isolation of the PEI/Pt NPs is quite good in the colloidal solution. It can be found that the majority of the Pt NPs have a nearly isometric morphology with very narrow size distribution in the image, and only a very few aggregated particles were observed. Figure 2b displays a high-resolution TEM (HRTEM) image. The spacing of lattice fringes measured from the image is 0.25 nm, which is consistent with the (111) interplane spacing of face-centered-cubic Pt NPs. The inset image shows a representive diffraction pattern obtained from fast Fourier transform (FFT) analysis of that particle. The HRTEM image shows that the photoreduced Pt NPs are well ordered at the atomic scale.

3.2. Characterization of PEI/Pt NPs by Cyclic Voltammetry (CV). ***Deposition of Pt NPs on Glassy Carbon Electrodes.*** The catalytic activity of Pt NPs is generally affected by their size, shape, and stabilizing agents controlled by preparative conditions. Many kinds of polyelectrolyte assemblies on electrodes have been studied (43). Among them, PEI is a polyelectrolyte that has been used widely for the preparation of multilayer assemblies, yielding novel multifunctional materials. The procedure in this study for polyelectrolyte coating of the electrode with PEI is based on solvent evaporation. The PEI/Pt NP solution was applied directly to the glassy carbon surface. After the solvent evaporated, the PEI coating layer was irradiated by UV light. It has been shown that γ-irradiation or UV radiation can generate free radicals on the polymer chains, which react to covalently cross-link the chain (44). Cross-linking combines the polymer chains into a continuous network extending over the entire electrode, which makes it intractable in that it is stable on the surface of the electrode and will not be soluble in the medium.

CV Profiles of PEI/Pt NPs. Figure 3 presents the cyclic voltammograms for PEI/Pt NP coating electrodes at different scan ranges in a 1 M H_2SO_4 solution. The PEI-coated electrode does not show any characteristic peak in the potential range shown (Figure S2 in the Supporting Information), whereas the PEI/Pt NP coating electrodes display the characteristic voltammetric profile of Pt surfaces (45): hydrogen adsorption−desorption, the double layer, and formation and removal of Pt surface oxides. These features are in good agreement with the CV curves for other Pt electrodes (46). This demonstrates that the voltammetric features of Pt NP electrodes are due to the presence of Pt in PEI on the electrode. Hydrogen underpotential (H_{upd}) deposition is very sensitive to the crystallographic orientation of the Pt surface (47). The adsorption peaks of hydrogen are distinctly resolved when the potential was scanned to the region of oxide formation, while when the potential was scanned below the oxide formation region, the adsorption peaks of hydrogen are not well resolved (Figure 3b). The corresponding hydrogen adsorption−desorption peaks H_{A1} and H_{D1} are associated with the Pt(110) crystal plane, and the hydrogen adsorption−desorption peaks H_{A2} and H_{D2} are associated

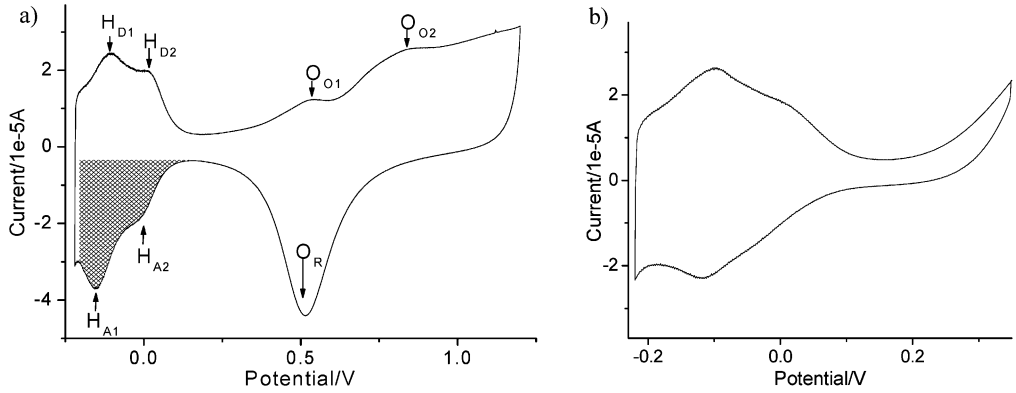

FIGURE 3. CV of the as-prepared PEI/Pt NP-coated electrode. Supporting electrolyte: nitrogen-saturated 1 M H_2SO_4. Scan rate: 20 mV s^{-1}. Electrode area: 0.07 cm^2. (a) Potential between −0.22 and 1.2 V. (b) Potential between −0.22 and 0.35 V.

with the Pt(100) crystal plane (36). The broad hydrogen adsorption below the Pt(110) and Pt(100) peaks possibly indicates the presence of Pt(111) sites. Resolved hydrogen adsorption states at the PEI/Pt NPs assembled on the electrode are a significant signal because they indicate that PEI is a good capping agent that does not block H_{upd} catalytic sites, while in the case of a PVP-mediated Pt colloidal, H_{upd} states cannot be resolved (29). The O_{O1} and O_{O2} peaks show typical Pt oxidation at high potential, while peak O_R is associated with the reduction of platinum oxide. This is further evidence of the presence of Pt at the electrode surface (48). It is concluded that the Pt NPs have accessible, active surfaces.

The catalytic activity of Pt NPs was evaluated by its active surface area. The active area of Pt NPs can be estimated by the hydrogen underpotential deposition. This area is calculated by integrating the cathodic current for the hydrogen adsorption reaction, correcting for the "double-layer" charging current (49) (as shown in the net shaded region in Figure 3a). A reported clean polycrystalline Pt electrode charge density of 210 μC cm^{-2} was used, assuming adsorption of one H atom per Pt atom (50). The area of the electrochemically accessible NPs was calculated to be 1.32 cm^2. The roughness factor (*f*), defined as the ratio of the true active surface area to the apparent geometric area, gives a value of about 20.

3.3. Electrocatalytic Activity of MOR. Pt NPs have good catalytic activity and stability for the electrochemical oxidation of methanol in the acidic environment of DMFCs (3). The catalytic properties of PEI-mediated Pt were studied by CV. Figure 4 presents the CVs obtained from the oxidation of methanol at PEI/Pt NP-coated electrodes in 1 M H_2SO_4 containing 2 M methanol. Voltage sweeps were scanned in the range of 0−1 V at a rate of 20 mV s^{-1}. A well-defined symmetric anodic peak for the oxidation of methanol at 0.66 V in the forward scan is apparent. In the reverse sweep direction, an anodic reverse peak was recoded at 0.47 V. This reverse anodic peak is attributed to the removal of surface-adsorbed, incompletely oxidized intermediate species generated during the oxidation of methanol, mainly CO. The peak currents at 0.66 and 0.47 V, which are consistent with that reported in the literature (48), are not observed at the pure PEI electrode (Figure S3 in the Supporting Information), demonstrating that the Pt NPs are responsible for the electrocatalytic activity.

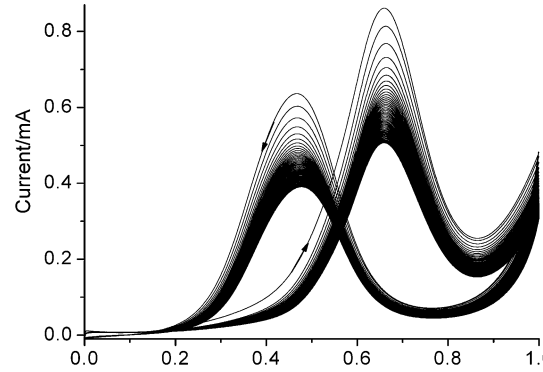

FIGURE 4. 50 consecutive cycle scans of methanol oxidation obtained from a PEI/Pt NP-coated electrode with a scan rate of 20 mV s^{-1} in 1 M H_2SO_4 and 2 M methanol at 298 K. The peak current decreases with the number of scans. The voltammograms were recorded at 2 s intervals.

Electrooxidation of methanol is a complicated chemical reaction. Even after several decades of study, the mechanism of the oxidation of methanol is still not completely understood. Several reaction mechanisms have been proposed (51). Spectroscopic studies (52) indicate that methanol molecules are first absorbed on the surface of Pt and disassembled as intermediates such as $Pt(CHO)_{ads}$ and $Pt(CO)_{ads}$; H_2O is absorbed to the surface of Pt as intermediate $Pt(OH)_{ads}$, which reacts with carbonaceous intermediates to give CO_2, producing the stripping peak in the backward scan. It is generally agreed that the most abundant surface intermediate is CO, which can poison the catalyst. The ratio of the magnitude of the anodic peak current in the forward sweep to the reverse sweep has generally been used to evaluate catalyst tolerance to intermediate species accumulation on the surface of the electrode (53). The higher the ratio of the forward anodic peak current to the backward anodic peak current (I_f/I_b), the more methanol is oxidized to carbon dioxide, which means that the concentration of intermediate species on the electrode is relatively lower, thus a better tolerance to the poisoning (48). In our experiments, the ratio is about 1.3. This is much higher than those reported for most of the other Pt-based electrodes. For example, the ratio of 0.87 was reported with nanosized Pt on C (53). Such a high value indicates that most of the CO is

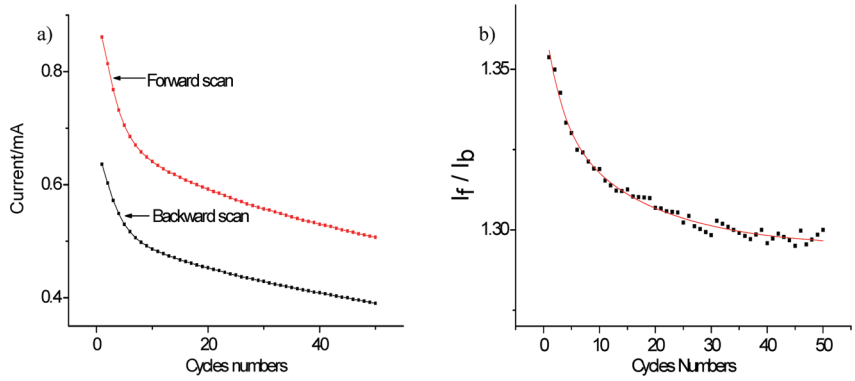

FIGURE 5. Long-term cycle stabilities of PEI/Pt NP-coated electrodes over 50 scans in nitrogen-saturated 1 M H_2SO_4 + 2 M CH_3OH at a scan rate of 20 mV s^{-1}: (a) variation of the forward and backward scan peak currents with the cycle number; (b) plot of I_f/I_b vs cycle number.

oxidized to CO_2 in the forward scan and that the PEI/Pt NP electrode does not undergo serious poisoning by the accumulation of CO. The onset potential for the oxidation of methanol in our experiments is about 0.1 V (Figure S4ain the Supporting Information), which is 0.3 V less positive than that for the bulk Pt electrode. (Figure S4b in the Supporting Information shows a CV comparison of PEI/Pt NPs with Pt electrodes. Both of them were recorded in 1 M H_2SO_4 containing 2 M CH_3OH at 20 mV/s.) The onset potential for the oxidation of methanol on our PEI/Pt NP-coated electrode is also much lower than those of the other Pt-based NP-based electrodes. For example, Geng and Lu (54) studied the onset potential of methanol electrooxidation for various Pt-based multicomponent electrocatalysts, and most onset potentials of their catalysts are in the range of 0.12−0.39 V; the onset potential on iridium (Ir)/Pt NP-based (55) and nanoporous Pt network (14) electrodes was observed at 0.2 V; it was also shown that the onset potential of CNT/Pt NP electrodes (56) was 0.2 V. Although such a comparison is not very precise because the catalytic activity is related to many factors such as the preparation technique, surface area, particle size and distribution, pretreatment, etc., the low onset potential and larger I_f/I_b ratios indicate that PEI/Pt NPs show superior electrocatalytic activity for methanol oxidation and good tolerance to CO poisoning.

In our study, the peak current in the first forward scan at 0.66 V is 0.861 mA. On the basis of the geometric electrode surface of 0.07 cm^2, we obtain a current density of 12.3 mA cm^{-2} for 2 M methanol (scan rate of 20 mV s^{-1}) on the Pt NP-coated electrode with a very low Pt loading. For comparison, Liang et al. (29) found that PVP-coated Pt NPs produce almost no response to methanol with no oxidative or hysteresis phenomena observed. Their work indicates that the poor signal arising from the PVP-stabilized NPs can be attributed to the presence of a strong capping agent on the Pt NP surface, inhibiting the particles' catalytic properties. The strong affinity of PVP for the Pt NPs hinders the diffusion of methanol to the Pt surface and thus inhibits electron transfer from Pt. In contrast, PEI/Pt NPs show good catalytic properties for methanol oxidation. The reasons may be that the affinity of PEI for Pt is not as strong as that of PVP or that UV irradiation lessens the affinity of PEI with Pt. In any event, the homogeneous distribution of Pt NPs and small size are expected to produce high electrocatalytic activity.

It may also be instructive to compare our results with those of Nafion-stabilized Pt NPs (57). The peak current of Nafion-stabilized Pt NPs for methanol reduction is 12.31 mA cm^{-2} (1 M H_2SO_4 + 2 M CH_3OH under a scan rate of 100 mV s^{-1}; Pt loading of 56 μg cm^{-2}). The peak current of PEI-stabilized Pt NPs for methanol reduction is also 12.3 mA cm^{-2} but with a much lower scan speed and much lower loading (1 M H_2SO_4 + 2 M CH_3OH under a scan rate of 20m V s^{-1}; Pt loading of 9.1 μg cm^{-2}). This comparison indicates that PEI-mediated Pt NPs appear to have greater electrocatalytic activity than Nafion-stabilized Pt NPs.

The long-term stability of the Pt NP-coated electrode is particularly important for the development of DMFCs. The long-term stability of the electrode was tested by using the same electrode for 50 repetitive cycles. The forward and backward peak currents (Figure 4) on Pt NP-coated electrodes were measured as a function of the number of cycles, as shown in Figure 5a. It can be seen that the shape and peak potential of the curves show no evident changes, but the peak current decreases with increasing cycle number. The gradual decrease in the catalytic activity after successive cycles of potential scans could result from the consumption of methanol during the electrochemical oxidation reaction. A better measure of the stability comes from the ratio of the forward anodic peak current to the backward anodic peak current (I_f/I_b), calculated as a function of the number of cycles, as shown in Figure 5b. Only a 3.7% decrease in I_f/I_b was observed after 50 cycles, demonstrating that the electrode does not undergo serious deactivation by the oxidation/reduction product and still shows good catalyst tolerance to poisoning.

In order to understand more about the nature of the oxidation product, scans at different potential limits were obtained as shown in Figure 6. When the scan limit is higher than 1.2 V, a new shoulder peak appears at about 1.18 V, which is associated with the oxidation of carbonaceous species. The backward anodic peak potential and peak current density decrease. This is consistent with results from Pt/C and Pt/CNTs (48, 53). The ratio of I_f/I_b increasing with the anodic scan limit confirms that the reverse anodic peak

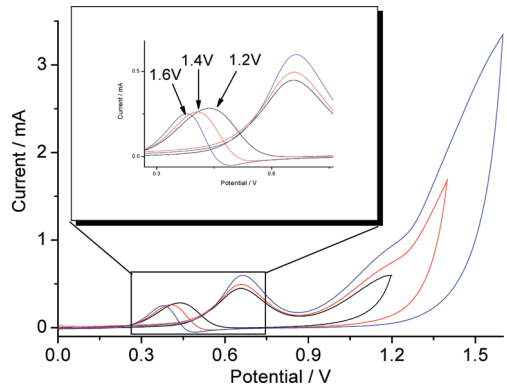

FIGURE 6. Cyclic voltammograms of methanol oxidation on a PEI/Pt NP-coated electrode at 20 mV s^{-1} in 1 M H_2SO_4 and 2 M CH_3OH with different potential scan limits labeled in the inset of the figure. The inset shows a magnified peak region.

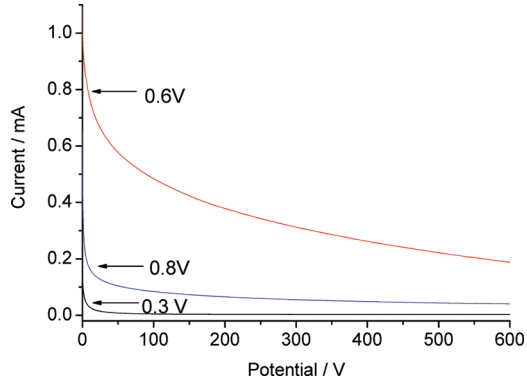

FIGURE 7. Chronoamperometry curves of a PEI/Pt NP-coated electrode for methanol oxidation recorded at 0.3, 0.6, and 0.8 V in 1 M H_2SO_4 and 2 M CH_3OH at 298 K.

current is associated with the residual carbon species on the Pt NP-coated electrode.

Chronoamperometry scans were measured at different potentials for 600 s on the Pt NP-coated electrode, and the results are shown in Figure 7. It was found that the largest current occurs at 0.6 V (compared to 0.8 and 0.3 V), consistent with the above results from CV. The current gradually decreases with time because methanol is electrooxidized continuously and the concentration of methanol decreases with time.

CONCLUSION

In this study, we have demonstrated that monodisperse Pt NPs can be synthesized in a PEI aqueous solution by a photoreduction method. The results obtained from UV−vis spectroscopy and TEM clearly demonstrate the photoreduction of $PtCl_6^{2-}$ to Pt NPs and the photoreduction of $PtCl_6^{2-}$ complexes to Pt^0 metal particles via Pt^{2+}. Pt^0 metal formation apparently occurs only after almost all of $PtCl_6^{2-}$ converts to $PtCl_4^{2-}$. The reduction from $PtCl_6^{2-}$ to $PtCl_4^{2-}$ is a fast process, while the reduction of $PtCl_4^{2-}$ to Pt^0 metal particles is a slow process. PEI/Pt NPs can be assembled on the surface of a glassy carbon electrode and the electrocatalytic activity evaluated. Hydrogen adsorption states were observed and well resolved at as-prepared PEI/Pt NP assembled on electrode surfaces, without subjecting the NPs to decapping processes. The high current density, I_f/I_b value, and lower onset potential for methanol oxidation show that the PEI/Pt NPs exhibit excellent catalytic properties for MORs. They do not appear to be strongly sensitive to the accumulation of intermediate carbonaceous species on the surface, which leads to catalyst poisoning in fuel cells. The system is stable toward the oxidation of methanol. These results indicate that PEI is a good candidate to be used as a capping and reducing agent in the photoreduction of Pt NPs. At the same time, it can work as a good carrier to immobilize the NPs on the surface of the electrode. The presence of PEI in this system not only mitigates the CO poisoning of the Pt catalyst but also enhances the electrocatalytic activity and stability of the catalyst. A PEI-assisted photoreduction synthesis appears to be a promising method for the preparation of well-dispersed Pt NPs, and this method provides an attractive route to Pt catalysts with good electrocatalytic activity and reliable catalytic performance.

Acknowledgment. This work used the Central Analytical Facility, which is supported by The University of Alabama. The authors acknowledge the MRSEC Program of the National Science Foundation under Award DMR-0213985. The authors thank Dr. Shanlin Pan and Zhufang Liu for fruitful discussions.

Supporting Information Available: XPS spectrum of the Pt 4f region of the as-prepared NPs (Figure S1), CV of a PEI-coated electrode in nitrogen-saturated 1 M H_2SO_4 (Figure S2), CV of a PEI-coated electrode in a nitrogen-saturated H_2SO_4 mixture of 1 M H_2SO_4 and 2 M CH_3OH (Figure S3), and magnified CV in the oxidation of CH_3OH to show the onset potential and a comparison CV of PEI/Pt NP with a bulk Pt electrode (Figure S4). This material is available free of charge via the Internet at http://pubs.acs.org.

REFERENCES AND NOTES

(1) McGrath, K. M.; Prakash, G. K. S.; Olah, G. A. *J. Ind. Eng. Chem.* **2004**, *10*, 1063–1080.
(2) Acres, G. J. K. *J. Power Sources* **2001**, *100*, 60–66.
(3) Antolini, E.; Lopes, T.; Gonzalez, E. R. *J. Alloys Compd.* **2008**, *461*, 253–262.
(4) Vigier, F.; Rousseau, S.; Coutanceau, C.; Leger, J. M.; Lamy, C. *Top. Catal.* **2006**, *40*, 111–121.
(5) Kjeang, E.; Goldak, J.; Golriz, M. R.; Gu, J.; James, D.; Kordesch, K. *J. Power Sources* **2006**, *153*, 89–99.
(6) Zhdanov, V. P.; KaSerno, B. *Electrochem. Commun.* **2006**, *8*, 1132–1136.
(7) Lovic, J. *J. Serb. Chem. Soc.* **2007**, *72*, 709–712.
(8) Liu, H. S.; Song, C. J.; Zhang, L.; Zhang, J. J.; Wang, H. J.; Wilkinson, D. P. *J. Power Sources* **2006**, *155*, 95–110.
(9) Liu, Z.; Hu, J. E.; Wang, Q.; Gaskell, K.; Frenkel, A. I.; Jackson, G. S.; Eichhorn, B. *J. Am. Chem. Soc.* **2009**, *131*, 6924.
(10) Liu, Z. F.; Ada, E. T.; Shamsuzzoha, M.; Thompson, G. B.; Nikles, D. E. *Chem. Mater.* **2006**, *18*, 4946–4951.
(11) Yano, H.; Inukai, J.; Uchida, H.; Watanabe, M.; Babu, P. K.; Kobayashi, T.; Chung, J. H.; Oldfield, E.; Wieckowski, A. *Phys. Chem. Chem. Phys.* **2006**, *8*, 4932–4939.
(12) Ye, H.; Crooks, J. A.; Crooks, R. M. *Langmuir* **2007**, *23*, 11901–11906.
(13) Zhang, L.; Lee, K. C.; Zhang, J. J. *Electrochim. Acta* **2007**, *52*, 7964–7971.
(14) Ahmadi, T. S.; Wang, Z. L.; Green, T. C.; Henglein, A.; ElSayed, M. A. *Science* **1996**, *272*, 1924–1926.
(15) Elechiguerra, J. L.; Larios-Lopez, L.; Jose-Yacaman, M. *Appl. Phys. A: Mater. Sci. Process.* **2006**, *84*, 11–19.
(16) Siani, A.; Wigal, K. R.; Alexeev, O. S.; Amiridis, M. D. *J. Catal.* **2008**, *257*, 5–15.

(17) Li, J.; Liang, Y.; Xu, Q. C.; Fu, X. Z.; Xu, J. Q.; Lin, J. D. *J. Nanosci. Nanotechnol.* **2006**, *6*, 1107–1113.
(18) Chen, J. Y.; Herricks, T.; Xia, Y. N. *Angew. Chem., Int. Ed.* **2005**, *44*, 2589–2592.
(19) Maiyalagan, T. *J. Power Sources* **2008**, *179*, 443–450.
(20) Chen, C. W.; Takezako, T.; Yamamoto, K.; Serizawa, T.; Akashi, M. *Colloids Surf., A* **2000**, *169*, 107–116.
(21) Mizukoshi, Y.; Takagi, E.; Okuno, H.; Oshima, R.; Maeda, Y.; Nagata, Y. *Ultrason. Sonochem.* **2001**, *8*, 1–6.
(22) Wang, H. D.; Sun, X. Q.; Ye, Y.; Qiu, S. L. *J. Power Sources* **2006**, *161*, 839–842.
(23) He, B. L.; Chen, Y. X.; Liu, H. F.; Liu, Y. *J. Nanosci. Nanotechnol.* **2005**, *5*, 266–270.
(24) Einaga, H.; Harada, M. *Langmuir* **2005**, *21*, 2578–2584.
(25) Sastry, M.; Patil, V.; Mayya, K. S.; Paranjape, D. V.; Singh, P.; Sainkar, S. R. *Thin Solid Films* **1998**, *324*, 239–244.
(26) Sakamoto, Y.; Fukuoka, A.; Higuchi, T.; Shimomura, N.; Inagaki, S.; Ichikawa, M. *J. Phys. Chem. B* **2004**, *108*, 853–858.
(27) Luo, X. H.; Imae, T. *J. Mater. Chem.* **2007**, *17*, 567–571.
(28) Luo, Y. L.; Sun, X. P. *Mater. Lett.* **2007**, *61*, 2015–2017.
(29) Liang, H. P.; Jones, T. G. J.; Lawrence, N. S.; Jiang, L.; Barnard, J. S. *J. Phys. Chem. C* **2008**, *112*, 4327–4332.
(30) Kuo, P. L.; Chen, W. F.; Huang, H. Y.; Chang, I. C.; Dai, S. A. *J. Phys. Chem. B* **2006**, *110*, 3071–3077.
(31) Laschi, S.; Bulukin, E.; Palchetti, I.; Cristea, C.; Mascini, M. *Ingenierie et Recherche Biomedicales* **2008**, *29*, 202–207.
(32) Rubianes, M. D.; Rivas, G. A. *Electrochem. Commun.* **2007**, *9*, 480–484.
(33) Sun, X. P.; Dong, S. J.; Wang, E. K. *Polymer* **2004**, *45*, 2181–2184.
(34) Jena, B. K.; Raj, C. R. *J. Phys. Chem. C* **2008**, *112*, 3496–3502.
(35) Pan, M.; Tang, H. L.; Jiang, S. P.; Liu, Z. C. *J. Electrochem. Soc.* **2005**, *152*, A1081–a1088.
(36) Estephan, Z. G.; Alawieh, L.; Halaoui, L. I. *J. Phys. Chem. C* **2007**, *111*, 8060–8068.
(37) Tian, Z. Q.; Jiang, S. P.; Liu, Z. C.; Li, L. *Electrochem. Commun.* **2007**, *9*, 1613–1618.
(38) Harada, M.; Okamoto, K.; Terazima, M. *Langmuir* **2006**, *22*, 9142–9149.
(39) Harada, M.; Einaga, H. *Langmuir* **2006**, *22*, 2371–2377.
(40) Xie, H.; Gu, Y. L.; Ploehn, H. J. *Nanotechnology* **2005**, *16*, S492–S501.
(41) Knecht, M. R.; Weir, M. G.; Myers, V. S.; Pyrz, W. D.; Ye, H.; Petkov, V.; Buttrey, D. J.; Frenkel, A. I.; Crooks, R. M. *Chem. Mater.* **2008**, *20*, 5218–5228.
(42) Cameron, R. E.; Bocarsly, A. B. *Inorg. Chem.* **1986**, *25*, 2910–2913.
(43) Silva, C. P.; Carapuca, H. M. *Electrochim. Acta* **2006**, *52*, 1182–1190.
(44) De Castro, E. S.; Huber, E. W.; Villarroel, D.; Galiatsatos, C.; Mark, J. E.; Heineman, W. R.; Murray, P. T. *Anal. Chem.* **1987**, *59*, 134–139.
(45) Frelink, T.; Visscher, W.; Vanveen, J. A. R. *J. Electroanal. Chem.* **1995**, *382*, 65–72.
(46) Komanicky, V.; Menzel, A.; You, H. *J. Phys. Chem. B* **2005**, *109*, 23550–23557.
(47) Komanicky, V.; Menzel, A.; Chang, K. C.; You, H. *J. Phys. Chem. B* **2005**, *109*, 23543–23549.
(48) Lin, Y. H.; Cui, X. L.; Yen, C.; Wai, C. M. *J. Phys. Chem. B* **2005**, *109*, 14410–14415.
(49) Formo, E.; Peng, Z. M.; Lee, E.; Lu, X. M.; Yang, H.; Xia, Y. N. *J. Phys. Chem. C* **2008**, *112*, 9970–9975.
(50) Wang, J.; Swain, G. M. *J. Electrochem. Soc.* **2003**, *150*, E24–E32.
(51) Hogarth, M. P.; Ralph, T. R. *Platinum Met. Rev.* **2002**, *46*, 146–164.
(52) Miki, A.; Ye, S.; Senzaki, T.; Osawa, M. *J. Electroanal. Chem.* **2004**, *563*, 23–31.
(53) Liu, Z. L.; Ling, X. Y.; Su, X. D.; Lee, J. Y. *J. Phys. Chem. B* **2004**, *108*, 8234–8240.
(54) Geng, D. S.; Lu, G. X. *J. Phys. Chem. C* **2007**, *111*, 11897–11902.
(55) Chen, A. C.; La Russa, D. J.; Miller, B. *Langmuir* **2004**, *20*, 9695–9702.
(56) Girishkumar, G.; Vinodgopal, K.; Kamat, P. V. *J. Phys. Chem. B* **2004**, *108*, 19960–19966.
(57) Liu, Z.; Qun Tian, Z.; Ping Jiang, S. *Electrochim. Acta* **2006**, *52*, 1213–1220.

AM900471F